NANO LETTERS

2009
Vol. 9, No. 12
4128-4132

Experimental Investigation of Heat Conduction Mechanisms in Nanofluids. Clue on Clustering

J. W. Gao,[†,‡] R. T. Zheng,[‡,§] H. Ohtani,[||] D. S. Zhu,[†] and G. Chen*[,‡]

Key Laboratory of Enhanced Heat Transfer and Energy Conservation, Ministry of Education, School of Chemistry and Chemical Engineering, South China University of Technology, Guangzhou, Guangdong 510641, People's Republic of China, Department of Mechanical Engineering, Massachusetts Institute of Technology, 77 Massachusetts Avenue, Cambridge, Massachusetts 02139, Department of Key Laboratory of Radiation Beam Technology and Materials Modification of Ministry of Education, College of Nuclear Science and Technology, Beijing Normal University, Beijing 100875, People's Republic of China, and Materials and Nanotechnology Department, Research and Advanced Engineering, Ford Motor Company, Dearborn, Michigan 48121

Received July 22, 2009; Revised Manuscript Received October 12, 2009

ABSTRACT

Heat conduction mechanisms in nanofluids, fluids seeded with nanoparticles, have been extensively scrutinized in the past decades to explain some experimental observations of their enhanced thermal conductivity beyond the effective medium theory. Although many mechanisms such as Brownian motion, clustering, ballistic transport, and internanoparticle potential are speculated, experimental proof of any of the mechanisms has been difficult. Here, we investigate the mechanisms experimentally by thermal conductivity measurements and structural analysis for the same materials in both liquid and solid states. These studies strongly suggest that clustering holds the key to the thermal conductivity enhancement of nanofluids.

Over the past decade, nanofluids, suspensions with solid nanoparticles, have attracted increasing interest due to some experimental observation of their enhanced thermal conductivity beyond the predictions of the effective medium theory and their potential applications in energy technologies.[1−5] Mechanisms of the thermal conductivity enhancement in nanofluids remain unclear and are intensely debated. For example, the microconvection models attribute the thermal conductivity enhancement to the Brownian motion,[6−9] but other estimations show that Brownian motion effect is small.[10,11] Various clustering models have also been proposed, including clustering with microconvection or clustering with conduction.[12−16] Ballistic transport model based on the kinetic theory, and solid-layering around nanoparticles has also been studied.[12] Despite that some of experimental data can be fitted with the models, parameters used in many cases are way out of range. For example, the kinetic theory model requires nanoparticle mean free path to be in the order of centimeters in liquid,[17] and opposite conclusions have been drawn on the impact of Brownian motion on the thermal conductivity enhancement.[6−12] The lack of understanding in mechanisms also arises from disparate experimental results, as different groups report vastly different experimental results that are contradictory even when similar fluids and nanoparticles are used. As evidence, in a recent round-robin study of several different nanofluids with 33 groups participating worldwide, no extraordinary enhancement in thermal conductivity beyond conventional effective medium theory was observed at all.[18] A recent review[19] and its subsequent comment[20] further shows that the debate on thermal conductivity enhancement is not settled and new experiments are needed to understand the mechanisms.

In this letter, we experimentally explored the mechanism of thermal conductivity enhancement in nanofluids. Our strategy is to investigate the thermal conductivity in both the liquid and the solid states. In the solid state, the Brownian motion is frozen out. We further control the particle clustering formation through using different host materials. Our experiments strongly suggest that clustering holds the key for the thermal conductivity enhancement. When clusters formed, thermal conductivity even in the solid state can outperform the prediction of the homogeneous effective

* To whom correspondence should be addressed. E-mail: gchen2@mit.edu.
[†] South China University of Technology.
[‡] Massachusetts Institute of Technology.
[§] Beijing Normal University.
[||] Ford Motor Company.

10.1021/nl902358m CCC: $40.75
Published on Web 11/11/2009

medium model. On the basis of the experimental observation, a two-level effective medium model was developed to explain the experimental data in both the liquid and the solid state. Furthermore, the experiment points to the direction of improving nanofluids thermal conductivity.

We used alumina nanoparticles and two different host materials, hexadecane and hog fat. The alumina nanoparticles and *n*-hexadecane (n-$C_{16}H_{34}$) used were purchased from Sigma-Aldrich (99.5% purity). *N*-hexadecane (denoted as hexadecane hereafter) is a linear alkane with the melting temperature of 18 °C. Hog fat was extracted from hog meat and purified at least three times by filter papers. Hog fat is a fatty acid mixture consisting of saturated and unsaturated fatty acids with different melting points,[21] so it has a nonuniform melting point within the range of 25−30 °C. The difference between hot fat and hexadecane is that one is amorphous and the other is polycrystalline when they are frozen. As we will show later, the morphologies of the Al_2O_3 nanoparticles in the solid states in the two hosts are very different and consequently, the thermal conductivity behavior is also. The nanofluids were prepared by a two-step method. First, two droplets of stabilizer (Span-80, Fluka) were fully mixed with 30 mL of the base fluid (e.g., hog fat or hexadecane). We have measured the thermal conductivity of hexadecane with different weight fraction of Span-80. At 3 wt %, the thermal conductivity is reduced only 0.9%. Two droplets in 30 mL of base fluids (the fraction is less 0.1%) have no effect on the base fluid thermal conductivity, as confirmed by our measurement and in agreement with literature.[22] Second, alumina nanoparticles were dispersed into previous base fluids by high-energy ultrasound[23] to form a stable suspension.

Thermal conductivity of the suspension with alumina nanoparticles was measured using the transient hot wire method developed by Nagasaka and Nagashima.[24] We have used this method in the past,[23] including comparing it with optical measurement method[25] and round-robin test.[18] Measured thermal conductivity values of pure water and hexadecane are within 1% of literature values. We also analyzed further experimental uncertainties and determined that random uncertainties of the experiment are within 0.013%, and the systematic uncertainties (e.g., due to the hot wire length inaccuracy) is 1.1%. For the same type of material, the systematic uncertainty is equal since it is based on the same wire. We carried out experiments during the heating up and cooling down processes between 5−52 °C. A thermal bath with 1 °C accuracy was used to control temperature and the temperature range of the bath can be changed between 25−80 °C. The cooling process was done in the mixture of water and ice. Thermal conductivity value for a given temperature was the same within 0.2% during the heating and cooling cycle. Average data of the cooling and heating is presented.

Figure 1 shows thermal conductivity enhancement, defined as $(k_{nc} - k_b)/k_b$, where k_{nc} and k_b are the thermal conductivity of the nanocomposites and the base media (hexadecane and hog fat), respectively, as a function of temperature along with the predictions of the Maxwell−Garnet (MG) model based on the spherical nanoparticles without considering interfacial

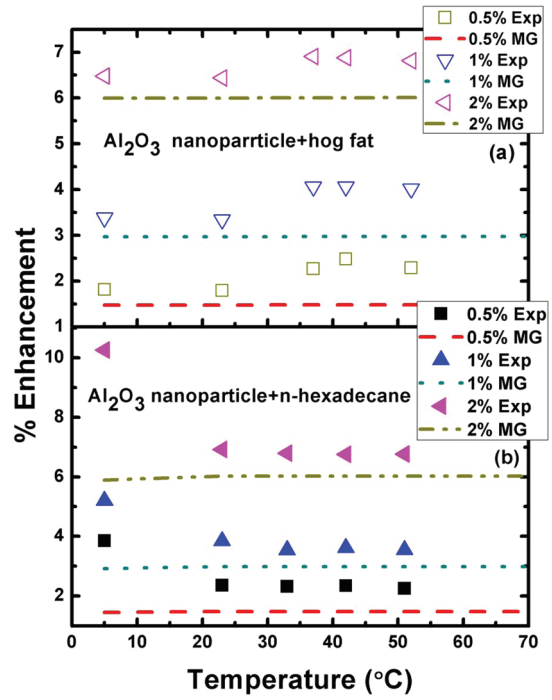

Figure 1. Thermal conductivity enhancement as a function of temperature for composites/nanofluids consisting of alumina in (a) hog fat and (b) hexadecane. Dots are experimental points, and lines are based on MG model assuming particles are uniformly distributed in the host media.

thermal resistance.[26] The thermal conductivity of the two different media shows different trends in the solid and the liquid states. For the hog fat, the thermal conductivity increases slightly with the phase changing from the solid state to the liquid state with a maximum difference of about 0.5% (in the percent thermal conductivity enhancement) from the prediction of the MG model. On the contrary, the thermal conductivity enhancement of the hexadecane-based composites is much larger in the solid state compared to the liquid state with a maximum difference of about 3.3% from the predictions of the MG model. The same trend can also be seen in Figure 2, which shows the thermal conductivity enhancement as a function of the alumina volume fraction. Hence, anomalous thermal conductivity enhancement beyond the MG theory can be observed not only in the liquid state, but also in the solid state. Clearly, in the solid state, Brownian motion should not play a major role and the microconvection mechanism can be excluded.

The different trends of hog fat and hexadecane-based nanocomposites/nanofluids in the solid and the liquid states can be explained by the microstructures of the nanoparticle in their perspective states. Transmission electron microscope (TEM) images of the nanoparticles are taken based on samples drawn from both liquid and solid phases. Alumina nanoparticle has a mean diameter of $d_p = 70$ nm (Figure 3a) by dynamic light scattering method with a polydispersity of 0.124. The ζ-potential of the alumina in water with a pH value of 7 was determined to be around 51 mV. In hog fat, the appearance of the nanoparticle aggregation shows no change before and after frozen as shown in Figure 3b,c due to hog fat is amorphous in solid state. On the contrary,

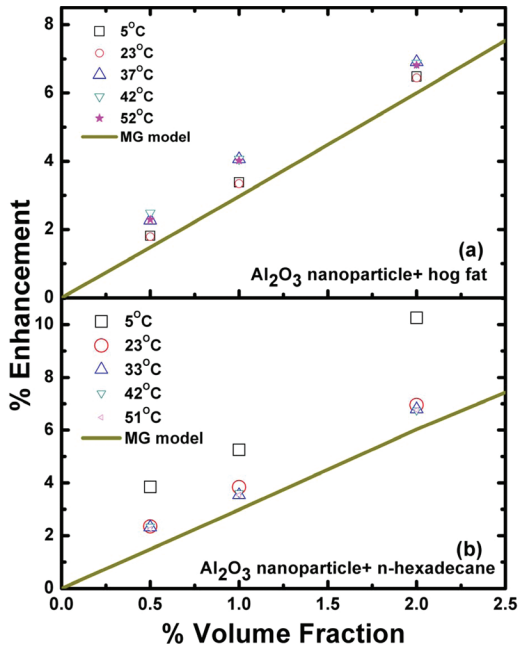

Figure 2. Thermal conductivity enhancement as a function of alumina volume fraction for composites/nanofluids consisting of alumina in (a) hog fat and (b) hexadecane. Dots are experimental points, and lines are based on MG model for particles uniformly distributed in the host media.

alumina nanoparticles agglomerate in an oriented fashion within the icelike hexadecane crystal structure upon freezing, as shown in Figure 3d,e. In taking TEM images of the solid state, a small hexadecane icicle is placed onto the TEM grid and the image is taken at room temperature. Icicles should be molten during the experiment. However, the TEM grids retained to some degree the clustering configuration of the nanoparticles in the solid-state. After remelting the solid-state composites into the liquid state, the continuous clusters break into the short clusters as shown in Figure 3f, and thermal conductivity returns to the values very close to these obtained before freezing as shown in Figure 4. The alumina nanoparticles aggregate into two kinds of clusters in the hexadecane crystals; one is a spherical cluster formed by larger diameter nanoparticles and the other is a "backbone" structure made of small diameter nanoparticles, forming rod-type of clusters that play a vital role in the thermal conductivity of the solid state. The mechanism of the nanoparticles aggregates in ice molds was detailed in ref 27 previously. The nanoparticles segregate into the grain boundaries of the ice crystals. The high aspect ratio backbone of the chainlike aggregates has a higher thermal conductivity, leading to a thermal conductivity enhancement larger than the prediction based on the assumption of spherical nanoparticles homogeneously dispersion in the medium. Although the formation of chainlike aggregation under a magnetic field was reported[28] before, the chains formed are along the field direction, while existing models are all on random three-dimensional structures likely existing in real nanofluids. Our experimental approach provides a fresh way to probe heat conduction mechanisms in nanofluids.

The larger enhancement is observed in the solid state than the liquid state in hexadecane due to clustering formation, and an opposite but weaker trend observed in hog fat led suggests that the effect of nanoparticle Brownian motion on thermal conductivity enhancement is much less than the effect of nanoparticle clustering. This is further supported by the observation that there is no temperature dependence in thermal conductivity enhancement at both solid and liquid states for the nanofluids composed by alumina particles and hog fat. Similarly, no temperature dependence was observed for alumina in hexadecane in nanofluids in the liquid state. We could not obtain more data points in the solid state for hexadecane due to limitations of our experimental system.

The traditional effective medium theory (EMT) model used for homogenization theories of well-dispersed composites fails to predict the thermal conductivity in the solid-state. Several clustering models have been developed in the past for the liquid state. Prasher et al. first combined clustering with Brownian motion[13] and then developed a three-level clustering model. As shown by TEM images, the spherical clusters are only a small part compared to the rode-type clusters (about 1:10 ratio from analysis of more than 10 TEM images). We evaluated the contribution of the larger spherical clusters on effective thermal conductivity using the MG model by assuming all the clusters within are spherical, and confirmed that the thermal conductivity of nanocomposites/nanofluids containing spherical clusters is similar to that of the uniformly dispersed system, even in a extreme case where all the nanoparticles belong to the spherical clusters. Hence, spherical clusters cannot explain the experimental data. Our analysis thus focused on the rod-type clusters. On the basis of the TEM image, such clusters are not a single-particle chain, but consist of several particles in the direction perpendicular to the chain. We can estimate the thermal conductivity of the rod using the Bruggeman model of effective thermal conductivity,[29] which is particularly suited to the composites with high concentration additives[30]

$$\phi_{c\_p}\left(\frac{k_p - k_c}{k_p - 2k_c}\right) + (1 - \phi_{c\_p})\left(\frac{k_b - k_c}{k_b - 2k_c}\right) = 0 \qquad (1)$$

where k_p, k_b, and k_c are the thermal conductivity of the nanoparticle, the base medium and the cluster (or rod, in this case), respectively, and ϕ_{c_p} denotes the volume fraction of the nanoparticle within the clusters.

Assuming the clusters as rods with effective thermal conductivity calculated from eq 1, we can further calculate the thermal conductivity of the solid or liquid nanocomposites. We use model by Nan[31] for random oriented ellipsoidal inclusions by approximating the rod into ellipsoids

$$\frac{k_{nc}}{k_b} = \frac{3 + \phi_c(2\beta_{11}(1 - L_{11}) + \beta_{33}(1 - L_{33}))}{3 - \phi_c(2\beta_{11}L_{11} + \beta_{33}L_{33})} \qquad (2)$$

where k_{nc} is the thermal conductivity of the solid or liquid nanocomposite, ϕ_c is the volume fraction of the clusters in the composite. The relationship among ϕ_c, ϕ_{c_p}, and ϕ_p are $\phi_c = \phi_p/\phi_{c\_p}$ due to the particle number conservation, where ϕ_p is volume fraction of nanoparticles in composites. In eq

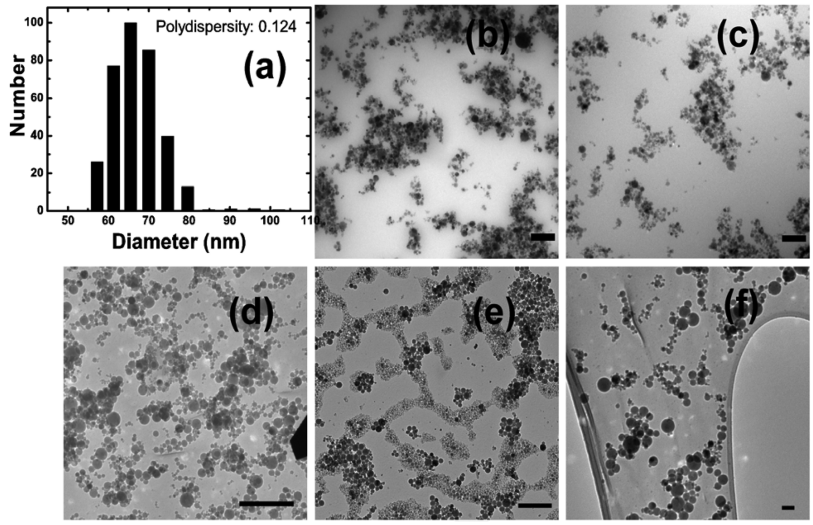

Figure 3. (a) Particles size distribution of alumina in hexadecane by the DLS method. (b) TEM image of alumina in hog fat suspension before frozen, (c) alumina in hog fat composite after frozen, (d) alumina in hexadecane suspension before frozen, (e) alumina in hexadecane after frozen, (f) alumina in hexadecane suspension after remelting. The scale bar of (f) is 100 nm, and the others are 500 nm.

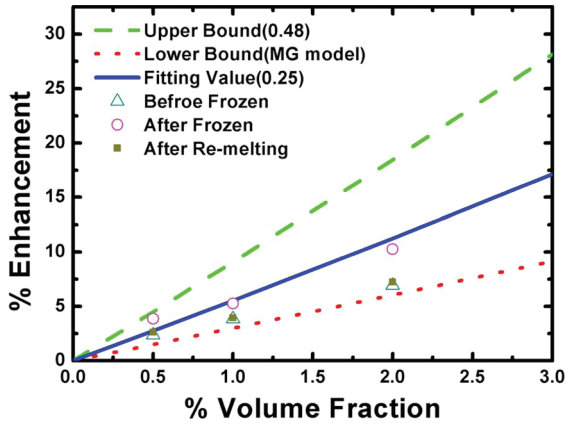

Figure 4. Model analysis of thermal conductivity enhancement of hexadecane based composites/nanofluids. Here, the upper bound of the thermal conductivity enhancement is calculated with a particle packing density around 0.48 within nanoparticle clusters; the lower bound is predicted by the homogeneous MG model. The experimental value is fitted using a volume fraction of 25% and a cluster length to diameter ratio 5.

2, $L_{11} = 0.5Q^2/(Q^2 - 1) - 0.5Q \cosh^{-1} Q/(Q^2 - 1)^{1.5}$, $L_{33} = 1 - L_{11}$, $\beta_{11} = (k^c_{11} - k_b)/(k_b + L_{11}(k^c_{11} - k_b))$, and $\beta_{33} = (k^c_{33} - k_b)/(k_b + L_{33}(k^c_{33} - k_b))$, where $Q = L/R$ denotes aspect ratio of rod-type clusters (L and R are rod length and rod radius, respectively). $k^c_{11} = k_c/(1 + rL_{11}k_c/k_b)$, and $k^c_{33} = k_c/(1 + rL_{33}k_c/k_b)$, where $r = (2 + 1/Q)R_{Bd}k_b/d_p$ ($Q > 1$), and R_{Bd} is the thermal boundary resistance. We do not know exact values of thermal boundary resistance between Al_2O_3 and liquids used. However, past experiments of liquid−solid interfaces gave thermal boundary resistance values in the range of 2×10^{-9} m^2·K/W and 2×10^{-8} m^2·K/W.[32,33] In this work, the order of magnitude of 10^{-9} m^2·K/W was used. We found that the thermal boundary resistance does not have significant impact on the thermal conductivity of the effective medium.

Figure 4 shows the predictions of the above model along with the experimental value as a function of the volume fraction of the nanoparticles for hexadecane based nanocomposites. As detailed in ref 27, clusters are formed by the process of the solidification of the liquid, and the particle density (ϕ_{c_p}) is dependent on the pressure of grain boundary. Since our TEM image was taken at room temperature after the hexadecane icicles melt, the volume fraction of nanoparticles in clusters in the solid state is hard to determine exactly. According to the model prediction, the thermal conductivity of the nanocomposites/nanofluids peaks when the nanoparticle volume fraction within clusters reaches 0.48, although the maximum packing density (ϕ_{c_p}) can be as large as 0.74. This is because as more spheres are packed densely to increase the cluster thermal conductivity, the number of clusters decreases. We hence plotted in Figure 4 the effective thermal conductivity at the particle packing density of 0.48 within the clusters. The lower bound shown in the figure is predicted by the homogeneous MG model. Both the liquid and the solid-state data are within these bounds. For the solid-state case, we can fit the experimental results using a nanoparticle volume fraction of 0.25 within the clusters and a cluster length to diameter ratio of 5 based on the statistical analysis of more than 10 TEM images. We should point out that presently, large uncertainties exist in both the rod length and the volume fraction, and these are not to be taken as exact values. The thermal conductivity enhancement of the composites in the liquid state at room temperature is only slightly above the MG model. When the solid state composite was remelted into the liquid state, the measured thermal conductivity restores the initial value before freezing. The clusters can still be observed as shown in Figure 3f, but it is not continuous and broke into short clusters. We can explain the experimental data on liquid by assuming a rod aspect ratio about 2.

In conclusions, our results indicate that the Brownian motion of nanoparticles is not the main cause of the thermal conductivity enhancement. Rather, nanoparticle clustering appears to be a key contributor. Our study has provided a

strategy for achieving nanofluid systems with high thermal conductivity. One should look for nanoparticles with high thermal conductivity and easy to form (nonspherical) clustering configurations, or nanoparticles with directional high thermal conductivity values.

Acknowledgment. We would like to thank S. Shen, K. Collins, Y. Zhang, A. Henry, X. Chen, D. Kraemer, and Q. Hao for their helpful discussion during the course of this work. This work is supported by Ford-MIT alliance and NSF CBET-05-06830. J.W.G. and R.T Z. also gratefully acknowledge partial financial support from China Scholarship Council (CSC).

References

(1) Das, S. K.; Choi, S. U.; Yu, W.; Pradeep, T. *Nanofluids: Science and Technology*; Wiley-InterScience: Hoboken, NJ, 2007.
(2) Lee, S.; Choi, S. U. S.; Li, S.; Eastman, J. A. *ASME J. Heat Transfer* **1999**, *121*, 280.
(3) Choi, S. U. S. *ASME J. Heat Transfer* **2009**, *131*, 033106.
(4) Penas, J. R. V.; de Zarate, J. M. O.; Khayet, M. *J. Appl. Phys.* **2008**, *104*, 044314.
(5) Vladkov, M.; Barrat, J. L. *Nano Lett.* **2006**, *6*, 1224.
(6) Jang, S. P.; Choi, S. U. S. *Appl. Phys. Lett.* **2004**, *84*, 4316.
(7) Prasher, R.; Bhattacharya, P.; Phelan, P. E. *Phys. Rev. Lett.* **2005**, *94*, 025901.
(8) Krishnamurthy, S.; Lhattacharya, P.; Phelan, P. E.; Prasher, R. S. *Nano Lett.* **2006**, *6*, 419.
(9) Yang, B. *ASME J. Heat Transfer* **2008**, *130*, 042408.
(10) Eapen, J.; Williams, W. C.; Buongiorno, J.; Hu, L. W.; Yip, S.; Rusconi, R.; Piazza, R. *Phys. Rev. Lett.* **2007**, *99*, 095901.
(11) Evans, W.; Fish, J.; Keblinski, P. *Appl. Phys. Lett.* **2006**, *88*, 093116.
(12) Keblinski, P.; Phillpot, S. R.; Choi, S. U. S.; Eastman, J. A. *Int. J. Heat Mass Transfer* **2002**, *45*, 855.
(13) Prasher, R.; Evans, W.; Meakin, P.; Fish, J.; Phelan, P.; Keblinski, P. *Appl. Phys. Lett.* **2006**, *89*, 143119.
(14) Xuan, Y. M.; Li, Q.; Hu, W. F. *AIChE J.* **2003**, *49*, 1038.
(15) Gharagozloo, P. E.; Eaton, J. K.; Goodson, K. E. *Appl. Phys. Lett.* **2008**, *93*, 103110.
(16) Prasher, R.; Phelan, P. E.; Bhattacharya, P. *Nano Lett.* **2006**, *6*, 1529.
(17) Kumar, D. H.; Patel, H. E.; Kumar, V. R. R.; Sundararajan, T.; Pradeep, T.; Das, S. K. *Phys. Rev. Lett.* **2004**, *93*, 144301.
(18) Buongiorno, J.; Venerus, D. *J. Appl. Phys.,* in press; see also, the International Nanofluid Properties Benchmark Exercise (INPBE) Web site: http://mit.edu/nse/nanofluids/benchmark/index.html. Access date February 1, 2009.
(19) Keblinski, P.; Prasher, R.; Eapen, J. *J. Nanopart. Res.* **2008**, *10*, 1089.
(20) Murshed, S. M. S. *J. Nanopart. Res.* **2009**, *11*, 511.
(21) Guillén, M.; Cabo, N. J. *Am. Oil Chem. Soc.* **1997**, *74*, 1281.
(22) Han, Z. H.; Yang, B.; Kim, S. H.; Zachariah, M. R. *Nanotechnology* **2007**, *18*, 105701.
(23) Garg, J.; Poudel, B.; Chiesa, M.; Gordon, J. B.; Ma, J. J.; Wang, J. B.; Ren, Z. F.; Kang, Y. T.; Ohtani, H.; Nanda, J.; McKinley, G. H.; Chen, G. *J. Appl. Phys.* **2008**, *103*, 074301.
(24) Nagasaka, Y.; Nagashima, A. *J. Phys. E* **1881**, *14*, 1435.
(25) Schmidt, A. J.; Chiesa, M.; Torchinsky, D. H.; Johnson, J. A.; Nelson, K. A.; Chen, G. *J. Appl. Phys.* **2008**, *103*, 083529.
(26) Maxwell, C. J. *Electricity and Magnetism*; Oxford: Clarendon, 1873.
(27) Deville, S.; Saiz, E.; Nalla, R. K.; Tomsia, A. P. *Science* **2006**, *311*, 515.
(28) Philip, J.; Shima, P. D.; Raj, B. *Appl. Phys. Lett.* **2007**, *91*, 203108.
(29) Bruggeman, D. A. G. *Ann. Phys. (Leipzig)* **1935**, *24*, 636.
(30) Wang, B. X.; Zhou, L. P.; Peng, X. F. *Int. J. Heat Mass Transfer* **2003**, *46*, 2665.
(31) Nan, C. W.; Birringer, R.; Clarke, D. R.; Gleiter, H. *J. Appl. Phys.* **1997**, *81*, 6692.
(32) Ge, Z. B.; Cahill, D. G.; Braun, P. V. *Phys. Rev. Lett.* **2006**, *96*, 186101.
(33) Schmidt, A. J.; Alper, J. D.; Chiesa, M.; Chen, G.; Das, S. K.; Hamad-Schifferli, K. *J. Phys. Chem. C* **2008**, *112*, 13320.

NL902358M